

Structure of the medium formed in heavy ion collisions

J. R. Alvarado García,^a D. Rosales Herrera,^a A. Fernández Téllez,^a Bogar Díaz,^{b,c,d} and J. E. Ramírez^e

^a*Facultad de Ciencias Físico Matemáticas, Benemérita Universidad Autónoma de Puebla, Apartado Postal 165, 72000 Puebla, Puebla, Mexico*

^b*Departamento de Matemáticas, Universidad Carlos III de Madrid, Avenida de la Universidad 30, 28911 Leganés, Spain*

^c*Grupo de Teorías de Campos y Física Estadística. Instituto Gregorio Millán (UC3M), Unidad Asociada al Instituto de Estructura de la Materia, CSIC, Serrano 123, 28006 Madrid, Spain*

^d*Instituto de Ciencias Matemáticas (ICMAT), CSIC-UAM-UC3M-UCM, C. Nicolás Cabrera 13-15, 28049 Madrid, Spain*

^e*Centro de Agroecología, Instituto de Ciencias, Benemérita Universidad Autónoma de Puebla, Apartado Postal 165, 72000 Puebla, Puebla, Mexico*

E-mail: bodiazj@math.uc3m.es, jhony.ramirezcancino@viep.com.mx

ABSTRACT: We investigate the structure of the medium formed in heavy ion collisions using three different models: the Color String Percolation Model (CSPM), the Core-Shell-Color String Percolation Model (CSCSPM), and the Color Glass Condensate (CGC) framework. We analyze the radial distribution function of the transverse representation of color flux tubes in each model to determine the medium's structure. Our results indicate that the CSPM behaves as an ideal gas, while the CSCSPM exhibits a structural phase transition from a gas-like to a liquid-like structure. Additionally, our analysis of the CGC framework suggests that it produces systems that behave like interacting gases for AuAu central collisions at RHIC energies and liquid-like structures for PbPb central collisions at LHC energies.

KEYWORDS: Quark-gluon plasma; Structural phase transition; Color String Percolation Model; Color Glass Condensate; Heavy ion collisions

Contents

1	Introduction	1
2	Models	2
2.1	Color string percolation model	2
2.2	Core-shell-color string percolation model	3
2.3	Color glass condensate model	3
3	Simulation methods and data analysis	4
3.1	Color string percolation model	5
3.2	Core-shell-color string percolation model	5
3.3	Color glass condensate	7
4	Discussion and conclusions	11

1 Introduction

Quark-Gluon Plasma (QGP) is a state of matter that is believed to have existed in the early universe, shortly after the Big Bang. In this state, the quarks and gluons (which are normally confined within protons and neutrons) are liberated from their confinement and move freely in a hot and dense soup. The existence of QGP was first proposed in the 1970s [1–3] trying to understand the behavior of high-energy collisions between atomic nuclei.

It was not until the late 1990s, however, that experiments provided evidence for the creation of QGP. The collision of heavy ions, such as Au-Au at RHIC, produced a *liquid* made of quarks and gluons (the QGP), which exhibited a lower ratio of shear viscosity over entropy density than any other known material [4–6]. Its existence was later confirmed in Pb-Pb collisions at LHC [7–9]. Also, similar properties have been observed in other collisions, such as pp, pA collisions at LHC [10], as well as d-Au and ^3He -Au at RHIC [11].

Several models have been proposed in the literature to describe the quark-gluon plasma formation and its phenomenology. They are able to explain most of the experimental data, but not all. Two of the most popular approaches are the Color String Percolation Model (CSPM) [12–15] and the Color Glass Condensate model (CGC) [16, 17].

We are interested in studying the capacity of the two mentioned models to predict the liquid behavior of the QGP. To be precise, we analyze three models a) CSPM, b) the Core-Shell-Color String Percolation Model (CSCSPM) [18], which is a generalization of the CSPM, and c) CGC. One way to analyze the physical structure of a system is by examining the behavior of the radial distribution function (also referred to as the pair correlation function), denoted as $g(r)$. It explains the variation of the average particle count concerning the distance r from a given point. This function is a prevalent tool for evaluating packing structures and provides valuable data on the long-range correlations between particles and their organization [19]. The structure of the systems is revealed by $g(r)$ as follows: a) if it is featureless (flat

function) the system corresponds to an ideal gas structure, b) for a non-ideal gas the $g(r)$ possess a peak (a maximum) follows for a plain behavior, and c) for a liquid-like structure $g(r)$ exhibits several peaks (increasingly smaller).

In this work, we review the radial distributions function for the CSPM and the CSCSPM that was studied in [18], and analyze it for the CGC model. We present the basic features of the three mentioned models in section 2. Then, in section 3 we discuss the employed simulation methods and we analyze the behavior of $g(r)$ for the models of section 2. Finally, we give our conclusions in section 4.

2 Models

In this section, we present the general features of the CSPM, CSCSPM, and CGC models.

2.1 Color string percolation model

One of the main models used to describe the formation of quark-gluon plasma is the CSPM. It has successfully explained many of the experimental findings on collisions involving pp, pA, and AA interactions, including the azimuthal distributions of the resulting particles and the temperature dependence of the ratio between the shear and bulk viscosities over the entropy density [20, 21]. The CSPM is also able to predict the center of mass energy required for the QGP formation depending on the size of the systems [22].

The CSPM characterizes ion collision by the strong interaction between their constituent partons, which can be represented by color flux tubes extended in the beam axis direction, depicted as circular areas in the transverse plane. These objects, named strings, are represented by fully penetrable disks of radius $r \sim 0.2\text{-}0.3$ fm [12–14, 23]. The systems under this picture can be studied from percolation theory, where the overlapping between strings gives rise to different regions called color sources. The number of strings grows with the system's size, multiplicity, and energy, allowing the formation of a spanning cluster that marks the geometric phase transition and then the onset of the QGP formation.

Each individual color string has a certain area S_1 , color charge arbitrarily oriented \mathbf{Q}_1 with its corresponding color field intensity Q_1 , and produces particles in the midrapidity region with multiplicity μ_1 , and average squared transverse momentum $\langle p_T^2 \rangle_1$ [12–14]. Because of the random orientation of the color field, the resulting intensity of the color field for a color source, indexed by i , is proportional to the square root of the number of overlapped string n_i in the fraction of the string area $S^{(i)}/S_1$. Therefore, the obtained color field intensity is $Q^{(i)} = \sqrt{n_i} Q_1 S^{(i)}/S_1$ [12–14].

As a consequence of the color sum, the multiplicity and average squared transverse momentum of a color source is obtained via $\mu^{(i)} = \mu_1 Q^{(i)}/Q_1 = \sqrt{n_i} \mu_1 S^{(i)}/S_1$ and $\langle p_T \rangle^{(i)} = \langle p_T^2 \rangle_1 Q^{(i)}/Q_1 = \sqrt{n_i} \langle p_T^2 \rangle_1 S^{(i)}/S_1$. The sum of all contributions to a cluster of M color sources and n strings produces the total μ_n and $\langle p_T^2 \rangle_n$ of the cluster [12, 14]. Let us consider the two extreme cases of a cluster of n strings: on one hand, for the case of strings just touching each other, the total area covered by disks is the sum of the individual areas $S_n = nS_1$, and the same for the total multiplicity given by the sum of individual contributions $\mu_n = n\mu_1$, the average of p_T^2 match with the weighted sum of each string $\langle p_T^2 \rangle_n = n\mu_1 \langle p_T^2 \rangle / \mu_n = \langle p_T^2 \rangle_1$. On the other hand, the case of n strings fully overlapped leads to a total area $S_n = S_1$, and the only color source has the same area S_1 ; the observables $\mu_n = \sqrt{n} \mu_1$ and $\langle p_T^2 \rangle_n = \sqrt{n} \langle p_T^2 \rangle_1$.

correspond to the multiplicity and average of p_T^2 of a single color source with n overlaps, in this scenario it is found the maximal suppression for the multiplicity and the average of p_T^2 is maximally enhanced. This is consistent with the conservation of momentum relationship $n\mu_1 \langle p_T^2 \rangle_1 = \mu_n \langle p_T^2 \rangle_n$, that arises from the color sum rules established in the model [12, 14].

Note that a suppression effect naturally emerges depending on the spatial distribution of the strings, this effect is taken into account by the color reduction factor, $F(\eta)$, which depends on the fraction of the total area S occupied by n strings, the so-called string density parameter $\eta = nS_1/S$ [12, 14]. The color reduction factor drives the suppression of the multiplicity ($\mu = nF(\eta)\mu_1$) and the enhancement of the transverse momentum ($\langle p_T^2 \rangle = \langle p_T^2 \rangle_1 / F(\eta)$) [24]. It was found that $F(\eta)$ is a decreasing function, which means that as the string density increases, a colliding system produces fewer charged particles per string but with higher momentum. In this way, the color suppression factor emerges from the color string clustering process [22].

2.2 Core-shell-color string percolation model

In [18] was proposed a hybrid core-shell model together with the traditional CSPM, called CSCSPM. The idea was to take into account an excluding or repulsive interaction between strings. To be precise, the authors introduced a concentric region of exclusion into the strings (core region, the rest of the string area is called the shell region) of diameter $\lambda\sigma$ ($0 \leq \lambda \leq 1$, σ denotes the diameter of the strings). They also introduced a probability q_λ that determines whether a string can overlap with another string in its core region, classifying strings as soft or hard depending on whether they permit such overlaps. It is important to note that this overlap condition applies solely to core-core interactions, as core-shell and shell-shell overlaps are permitted.

In the same way that their predecessor, the CSCSPM model explains particle production in collision physics through the formation of string clusters (same strings as in the CSPM). Notice that the hard strings act as a fluid of hard disks of diameter $\lambda\sigma$, while the soft ones are still ideal particles. Moreover, the parameter q_λ modules the number of hard strings distributed in the system. However, the structures and phenomenology of the system depend on the combinations of both parameters. For example, if $\lambda = 1$ and $q_\lambda = 0$, the system recovers the picture of a fluid of hard disks [25], which may exhibit a liquid structure for densities above a particular string density. This condition prevents the formation of clusters, and then each string should produce charged particles individually, but on average, their transverse momentum squared will be the corresponding of one string divided by the multiplicity. This mechanism inhibits the formation of charged particles with higher transverse momentum. Also, if $q_\lambda = 0$, the model reproduces the continuum percolation of disks with hard cores [26, 27]. Finally, If $\lambda = 0$ or $q_\lambda = 1$, the system corresponds to traditional 2D continuum percolation [28, 29], which is the geometric picture of the CSPM.

It was found in Ref. [18] that combinations of parameter values exist such that, at the same time, allow the system the clustering of color strings and the formation of coordination shells, the main indications of the changes in the structure of the system.

2.3 Color glass condensate model

The CGC can provide the initial conditions needed to estimate the transport coefficients and bulk properties of the strong-interacting matter created in heavy ion collisions [30]. It is characterized by strong coherent gluon fields leading to parton saturation controlled by a

dynamically generated transverse momentum scale, the saturation scale Q_s [31–41]. The high gluon densities correspond to strong classical fields, and the quantum corrections to them are incorporated via nonlinear renormalization group equations. The nonlinear density-dependent terms in the CGC evolution equations can be identified as gluon recombination processes that saturate the increment in gluon densities below Q_s . Then, the value of Q_s sets the scale of gluon field fluctuations that can describe the bulk multiplicity and its fluctuations depending on the considered colliding system [42, 43]. The particle multiplicity distributions are intrinsically dependent on event-by-event fluctuations of the incoming nuclear wave functions.

In the framework of the CGC, to provide information about the systems’ characteristics it is used the Impact Parameter (IP) Glasma model, which combines the IP saturation dipole model [44] and nonlinear dynamics of the gluon fields [45, 46]. The Q_s^2 ’s distribution can be used to sample different color field configurations inside the proton according to the McLerran-Venugopalan (MV) model [47, 48]. The IP-Glasma model includes fluctuations in the nuclear and sub-nuclear position of static large- x color charges leading the gluon fields fluctuations that describe the dynamical small x modes in the CGC effective field theory [49, 50]. The different occupation probabilities of the QCD fields give rise to global fluctuations in observables such as the energy density in the transverse plane of the collision, which lead to fluctuations in the charged hadron flow harmonics through the dynamical evolution of the system [51]. It was proposed that in every event, the value of Q_s^2 at every point in the transverse plane fluctuates according to a probability distribution given by [52, 53]

$$P\left[\ln\left(\frac{Q_s^2}{\langle Q_s^2 \rangle}\right)\right] = \frac{1}{\sqrt{2\pi\varsigma^2}} \exp\left[-\frac{1}{2\varsigma^2} \ln^2\left(\frac{Q_s^2}{\langle Q_s^2 \rangle}\right)\right]. \quad (2.1)$$

This particular distribution gives rise to a skewed distribution of $Q_s/\langle Q_s \rangle$ around 1. We use the value of $\varsigma = 0.6$ reported in [54] to describe heavy ion collisions from AuAu to PbPb.

In addition to the skewness, the saturation scale Q_s also depends on the size and energy of the colliding nuclei. It was found that Q_s grows with the size of the colliding nuclei as $\sim A^{1/3}$ [47, 48, 55], where A is the nucleon number. Moreover, Q_s rises with the energy as the power law $\sim \sqrt{s}^\lambda$ (at midrapidity region) with $\lambda = 0.252$ [56]. For AuAu collisions at $\sqrt{s} = 130$ GeV, the saturation scale is taken to be $\langle Q_s^2 \rangle = 2$ GeV² [57]. Using the scaling laws described above, the saturation scale for AuAu central collisions at $\sqrt{s} = 200$ GeV and PbPb central collisions at $\sqrt{s} = 2760$ and 5020 GeV are estimated to be 2.23, 4.399, and 5.114 GeV², respectively. These values are used in the subsequent analysis of the heavy ion collisions.

3 Simulation methods and data analysis

In this section, we discuss the methodology used to determine the radial distribution functions and provide an introduction to the computer simulation basic notions of the models of interest. We also present the obtained results.

The radial distribution function $g(r)$ (also referred to as a pair correlation function or pair distribution function) determines the structure of the matter by analyzing the variations in the positions of its constituents, more precisely, in the average of the local density number at a distance r . Specifically, $g(r)$ describes the average local density of objects at a distance r from a reference object. In our simulations, we generate samples of the systems as square boxes of size $L = 8\sigma_o$, with σ_o being the characteristic diameter of the objects distributed on

the transverse plane of each model. Next, we generate suitable configurations of the system that satisfy the conditions of the corresponding model. Then, the radial distribution function is estimated as follows

$$g(r) = \frac{n(r)L^2}{N(2\pi\Delta r(r + 0.5\Delta r) + \pi\Delta r^2)}, \quad (3.1)$$

where $n(r)$ is the average number of objects at a distance between r and $r + \Delta r$ from a trial disk allocated on the center of the square box, and N is the number of objects distributed on the square box.

In the following subsections, we deeply discuss the peculiarities of the simulation and structures observed for the CSPM, CSCSPM, and CGC models. In order to compare the results of the different models, we compute $g(r)$ over the range of distances r/σ_o from 0 to 3.5, with increments of $\Delta r/\sigma_o = 0.035$.

3.1 Color string percolation model

As we explain in section 2, the CSPM considers strings like fully penetrable disks. This is equivalent to the image of a classical ideal gas and has to be reflected in the radial distribution. In this model, the simulations are performed accordingly to the two dimensional continuum percolation of disks. In this way, the color strings are uniform and randomly allocated in the square box without any conditions on the overlapping between them. After adding N disks, the radial distribution function is computed by using (3.1). This was previously analyzed in [18], and it was found that independently of the string density the $g(r)$ is a flat function. We show in Fig. 1 our results of $g(r)$ for the CSPM considering different string densities.

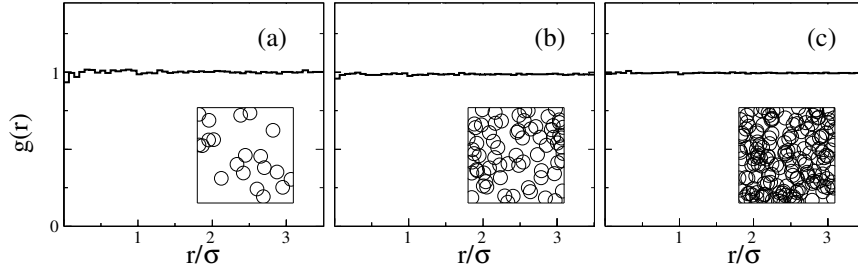


Figure 1. Radial distribution function for CSPM systems.

We must mention that other authors have also predicted the ideal gas behavior of the CSPM. For instance, in Refs. [58, 59] the authors studied the electrical and thermal conductivity of the QGP, using the CSPM, founding that the system agrees with an ideal gas. Also, in Ref. [60], a finite-size analysis of the speed of sound was performed, concluding that the CSPM corresponds to a mean-field theory.

3.2 Core-shell-color string percolation model

As discussed above, the CSPM only describes systems with an ideal gas structure because of the fully penetrable color strings. However, other structures (as nonideal gas or liquid-like)

may be observed if a repulsive interaction between the strings is introduced, as was done in the CSCSPM.

The CSCSPM configurations are generated by using the random sequential addition algorithm, in which disks are added one by one. At each step, a test string is randomly placed on the square box and designed as soft or hard. Then, according to the values of λ and q_λ , the test string is accepted if it, along with its neighbor strings, satisfies a valid configuration. Otherwise, the test string is rejected and a new test string is checked. This procedure is repeated until the system is filled with N strings. After generating the CSCSPM configuration, we measure its $g(r)$ using (3.1).

In Fig. 2, we show samples of core-shell-color string systems generated by using the aforementioned algorithm together with their corresponding radial distribution function, which is obtained as the average over 10^6 realizations.

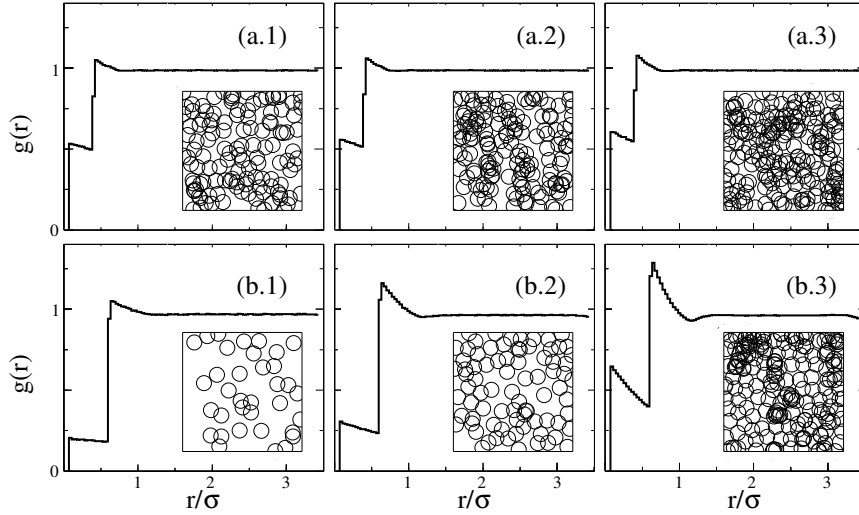


Figure 2. Samples of systems for the CSCSPM along with their corresponding radial distribution function. Note that in (b.2) and (b.3), we observe a transition from nonideal gas to liquid-like structures.

It is remarkable that the CSCSPM allows structures more complex than the ideal gas. In ref. [18] was found that exists values of λ and q_λ at which the systems have liquid-like structures, as shown in Fig. 2 (b.3). It is worth mentioning that the CSCSPM predicts values of λ and q_λ at which the structural and geometrical transitions occur almost simultaneously, with a difference of temperatures of 1 MeV. Figure 3 shows a sample of a CSCSPM system exhibiting a liquid-like structure together with the emergence of the spanning cluster.

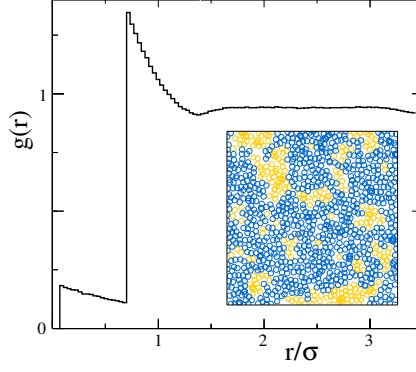


Figure 3. Sample of a system that shows a liquid-like structure together with the spanning cluster. This occurs with a difference in transition temperatures (configurational and geometric) lower than 1 MeV.

3.3 Color glass condensate

To analyze the structure of systems given by the CGC model, it is required to know the distribution of the saturation scale Q_s^2 , and the running coupling α_s , which provide the initial conditions of the distribution of gluons and their interaction. In this work, we consider that Q_s^2 fluctuates according to the Log-normal distribution given by Eq. (2.1). Then, the values of Q_s^2 are simulated via the normal distribution, that is, $Q_s^2 = \langle Q_s^2 \rangle e^x$, where x is a random number taken from a normal distribution $\mathcal{N}(0, 1)$, and $\langle Q_s^2 \rangle$ is the average value of Q_s^2 . The determination of $\langle Q_s^2 \rangle$ involves analyzing experimental data. We use the modified minimal subtraction scheme (\overline{MS}) to compute the values of α_s at zero order. Thus

$$\alpha_s(Q_s^2) = \frac{4\pi}{\beta_0 \ln(Q_s^2/\Lambda_{\text{QCD}}^2)}, \quad (3.2)$$

with $\beta_0 = 11 - 2n_f/3$, and Λ_{QCD}^2 being the QCD scale. For the estimation of β_0 we use the value of the flavor number $n_f = 3$, and $\Lambda_{\text{QCD}} = 0.332$ GeV [61]. Notice that Λ_{QCD} works as a cutoff for the values of Q_s since lower values of Q_s produce nonphysical values of α_s . In Fig. 4, we show a sample of Q_s values and the corresponding value of α_s computed using (3.2), together with their histograms.

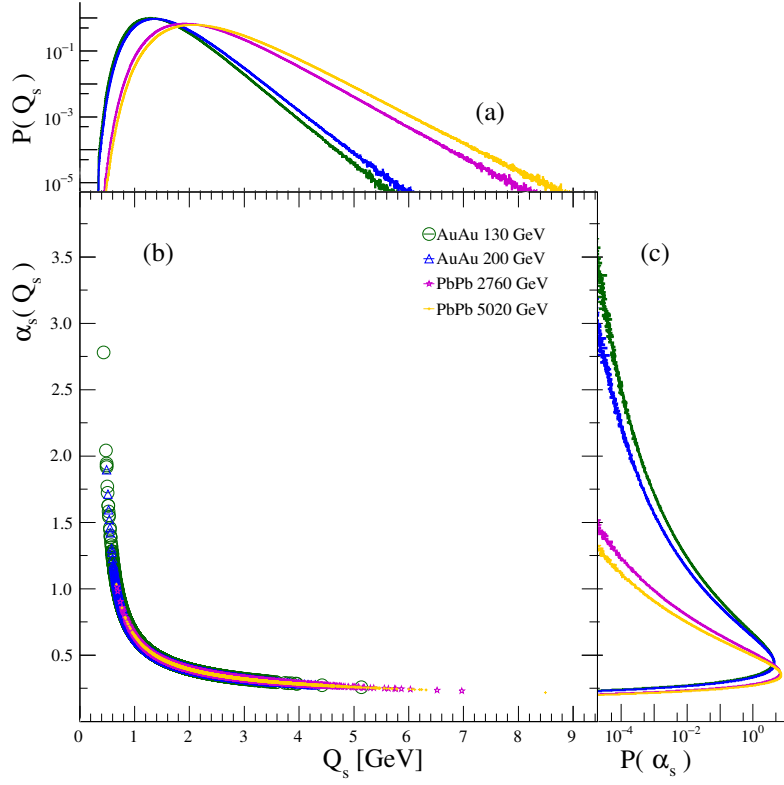


Figure 4. (a) Distribution of Q_s . (b) Sample of α_s -values as a function of Q_s . (c) Probability distribution function of α_s of the systems under study: AuAu at $\sqrt{s} = 130$ GeV (green lines and circles), AuAu at $\sqrt{s} = 200$ GeV (blue lines and triangles), PbPb $\sqrt{s} = 2760$ GeV (magenta lines and stars), and PbPb $\sqrt{s} = 5020$ GeV (yellow lines and crosses.).

In a nuclear collision, the Lorentz-contracted nuclei lead the partons to be confined to a flat region on the transverse plane. The occupied Glasma fields generated after the collisions are assumed to be proportional to the number of particles produced in a central pseudorapidity region at the saturation scale [56], which for low transverse momentum values is given by SQ_s^2/α_s [50, 57], where S is the overlapping area of nuclei. Taking these relations into account, the gluon density is

$$\rho = \frac{Q_s^2}{\alpha_s}. \quad (3.3)$$

Due to the saturation scale and coupling running are random variables, the gluon number density is also expected to exhibit random fluctuations, as depicted in Figure 5 (a). In consequence, the average minimum distance between gluons (computed from the gluon cross section) $\xi = 1/\sqrt{\rho}$ is also a random variable, as shown in Figure 5 (b).

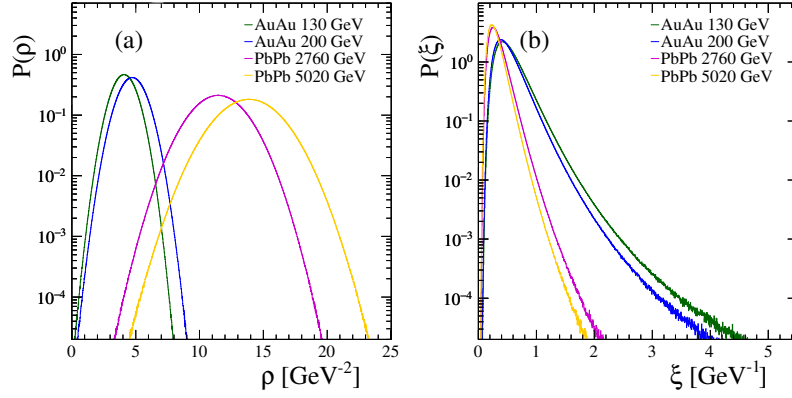


Figure 5. Discrete histograms for simulations. (a) the minimum distances between gluon centers and (b) the gluon density of the system.

For our simulations, we assume that the system is homogeneous and isotropic for AA central collisions (0-6% centrality) and we use as a length scale the average value of the gluon diameter, $\sigma = 2\langle r_g \rangle = 2\langle 1/\sqrt{\pi\rho} \rangle$. Following the same procedure as in the CSPM and the CSCSPM, we construct a square box of length side $L = 8\sigma$. Thus, the number of gluons in the system is $N_g = 64\sigma^2\rho$. Moreover, the probability of observing a system with exactly N_g gluons is calculated as usual

$$P(N_g) = \int_X P(\rho) d\rho \quad (3.4)$$

with X being the interval of ρ -values satisfying $\lfloor L^2\rho \rfloor = N_g$. Figure 6 (a) shows the distribution mass probability for the gluon number obtained from our simulations. This distribution takes into account all the fluctuations arising from the conditions of the CGC model and is relevant for computing the average of the radial distribution function.

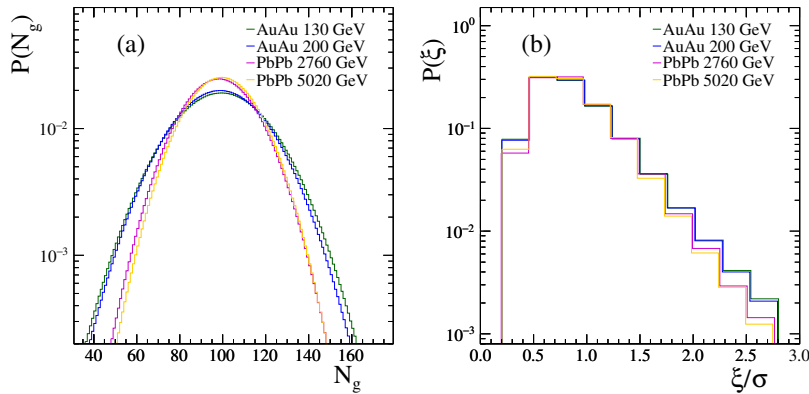


Figure 6. Used histograms for simulation (a) the number of gluons in the square and (b) classes of minimum distances among gluons normalized by the average diameter of a gluon.

To ensure valid configurations of gluon positions in our simulations, we use a criterion based on the probability density function of the minimal distance between nearest neighbor

gluons. Similarly to the number gluon N_g , we discretize that probability density function as follows. We consider the interval of ξ -values satisfying $P(\xi) > 0.01$. For the systems analyzed in this manuscript, this event has a probability of occurrence of 0.9968, 0.9971, 0.9985, and 0.9986, respectively. Then, we divide the interval into ten equally sized sub-intervals, where the probability of observing the i -subdivision is given by

$$P(i) = \int_{X_i} P(\xi) d\xi \Bigg/ \int_{\bigcup_{i=1}^{10} X_i} P(\xi) d\xi , \quad (3.5)$$

which produces the histograms depicted in Fig. 6 (b). This approach has two restrictions on the random variable ξ with zero probability, namely, (i) $\xi/\sigma < 0.2$, and (ii) $\xi/\sigma > 2.8$.

We initialize the simulation by allocating a trial disk at the center of a square box of side $L = 8\sigma = 16\langle r_g \rangle$. Then, we add $N - 1$ gluons one by one ensuring that the minimal distance between nearest neighbor gluons satisfies $0.2 < \xi/\sigma < 2.8$. After the addition of the N gluons, we *thermalize* the systems by moving an arbitrary gluon (except the trial gluon). For this test gluons, we generate a virtual random position on a neighborhood of the actual position and consider periodic boundary conditions. Thus, we calculate the distance ξ' to the nearest gluon. Next, we generate a uniformly random number on the interval $(0,1)$. The virtual position is accepted if $P(\xi') > x$, with $P(\xi')$ taken from the distribution on Fig. 6 (b). Otherwise, the position is rejected, and we repeat this methodology for another gluon. This procedure is repeated 10^4 moves per particle. After thermalization, we measure the number of particles $n(r, N)$ within a distance between r and Δr from the trial gluon with N particles in the system. In Fig. 7, we show samples of the systems after thermalization for AuAu and PbPb collisions at $\sqrt{s} = 130, 200$ GeV and $\sqrt{s} = 2760, 5020$ GeV, respectively. For consistency, we use the same parameters as those used for the CSPM and CSCSPM models to construct the plot of $g(r)$. We generate new valid configurations by moving a random gluon as described before and measure $n(r, N)$ again after 100 moves per gluon. Finally, the average of the number of gluons $n(r, N)$ after 10^4 simulation runs.

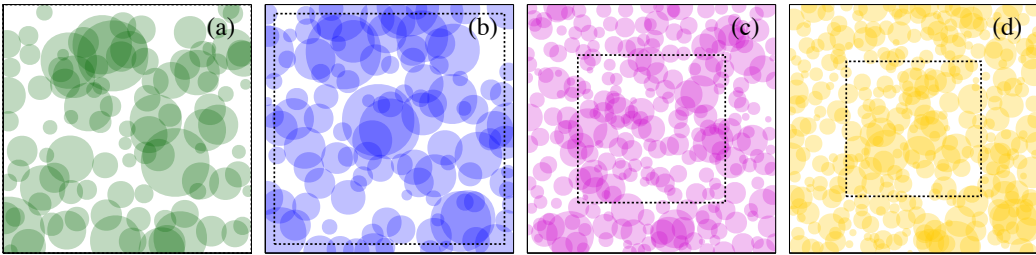


Figure 7. Samples of generated systems in the picture of the CGC after the thermalization for (a) AuAu collisions at $\sqrt{s} = 130$ GeV, (b) AuAu collisions at $\sqrt{s} = 200$ GeV, (c) PbPb collisions at $\sqrt{s} = 2760$ GeV, and (d) PbPb collisions at $\sqrt{s} = 5020$ GeV. These systems correspond to a square box of around 1fm^2 . The inner dashed square is the size of the simulated system for the purposes of the computation of the radial distribution function.

We recall that the number of gluons on the systems fluctuates for particular conditions of center of mass energy, centrality classification, pseudorapidity, and nucleon number, among

others. To account for these fluctuations, we determine the average of the radial distribution function as follows

$$g(r) = \sum_{N=N_{\min}}^{N_{\max}} \frac{L^2 n(r, N)}{N(2\pi\Delta r(r + 0.5\Delta r) + \pi\Delta r^2)} P(N) \bigg/ \sum_{N=N_{\min}}^{N_{\max}} P(N), \quad (3.6)$$

where $P(N)$ is the corresponding distribution of the number of gluons in Fig. 6 (a), $N_{\min} = \lfloor \langle N_g \rangle \rfloor - 3 \lfloor \sqrt{\text{var}(N_g)} \rfloor$, and $N_{\max} = \lfloor \langle N_g \rangle \rfloor + 3 \lfloor \sqrt{\text{var}(N_g)} \rfloor$. Figure 8 summarizes our results of the radial distribution function for AuAu and PbPb central collisions at $\sqrt{s} = 130, 200$ GeV and $\sqrt{s} = 2760, 5020$ GeV, respectively

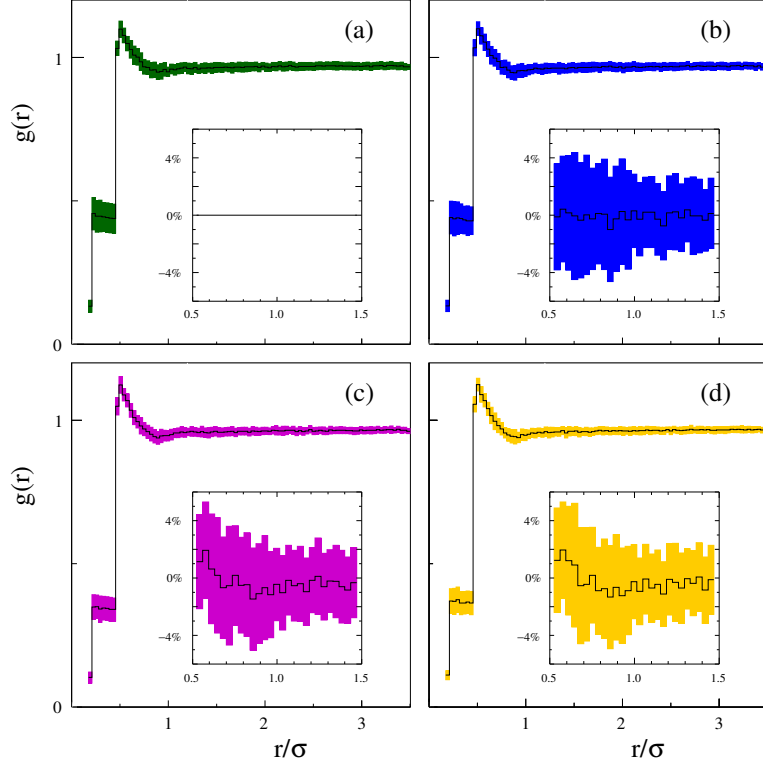


Figure 8. Radial distribution function of systems in the picture of the CGC for (a) AuAu collisions at $\sqrt{s}=130$ GeV, (b) AuAu collisions at $\sqrt{s}=200$ GeV, (c) PbPb collisions at $\sqrt{s}=2760$ GeV, and (d) PbPb collisions at $\sqrt{s}=5020$ GeV. The inner plots correspond to the percentage of deviation of the radial distribution function from the one obtained for AuAu collisions at $\sqrt{s}=130$ GeV.

4 Discussion and conclusions

In this paper, we have determined the structure of the medium formed in heavy ion collisions under the picture of the color string percolation model, the core-shell-color string percolation model, and the color glass condensate framework. We did this by analyzing the radial distribution function of the particular configuration of the distributed transverse representation of color flux tubes on each model: color strings in the CSPM and CSCSPM and gluons in the CGC.

It was found that the color string percolation model is structured as an ideal gas because of the fully overlapping condition of the string. By introducing a repulsive-like interaction between strings, the CSCSPM produces more complex structures, resembling a gas of interacting particles or a liquid-like fluid. The CSCSPM implements two new characteristics of the color strings: a concentric core region and a probability that a color string accepts core-core interaction. This implies a classification of the strings as soft and hard, which act like ideal particles or hard disks with diameter $\lambda\sigma$, respectively. A fine-tuning of the CSCSPM parameters (λ, q_λ) allows the systems to exhibit a structural phase transition at the same time as a geometrical phase transition. The former implies a transition from the gas structure to the liquid-like one, while the latter means the well accepted formation of the spanning cluster of color string, which can be interpreted as the onset of the quark-gluon plasma formation. The CSCSPM predicts conditions that both transitions occur almost simultaneously, with a difference of temperature of 1 MeV.

Other systems analyzed were those pictured by the color glass condensate. Here, we used the stochastic CGC framework that considers fluctuations on the saturation scale Q_s^2 . This also produces fluctuations in the running coupling, and then in all the characteristics of the CGC, such as the density, the size of gluons, and minimal distances between nearest neighbor gluons, among others. We found that the distribution of gluons for AuAu central collisions at RHIC energies (130 and 200 GeV) corresponds to a gas of interacting particles. On the other hand, for PbPb central collisions at LHC energies (2760 and 5020 GeV), we found evidence that the systems adopt a liquid-like structure. However, more simulations are needed to smooth the radial distribution function in Fig. 8 and apply a similar analysis on the $g(r)$ as described in Ref. [18]. It is worth noting that while we simulated homogeneous and isotropic system representations at the center of the transverse plane to the collision, the system may dilute at the edges, resulting in a radial distribution function that resembles that of a diluted interacting gas and eventually an ideal gas (flat function).

Acknowledgments

This work was partially supported by the grants PID2020-116567GB-C22 and CEX2019-000904-S funded by MCIN/AEI/10.13039/501100011033. Bogar Díaz acknowledges support from the CONEX-Plus programme funded by Universidad Carlos III de Madrid and the European Union's Horizon 2020 research and innovation programme under the Marie Skłodowska-Curie Grant Agreement No. 801538. This work was partially funded by Consejo Nacional de Ciencia y Tecnología (CONACyT-México) under the project CF-2019/2042, graduated fellowships grant numbers 645654 and 1140160, and postdoctoral fellowship grant number 289198. We thank Carlos Pajares for his valuable comments and fruitful discussions.

References

- [1] E. Shuryak, *Quark-gluon plasma and hadronic production of leptons, photons and psions*, *Phys. Lett. B* **78** (1978) 150.
- [2] L.D. McLerran and B. Svetitsky, *Quark liberation at high temperature: A monte carlo study of $su(2)$ gauge theory*, *Phys. Rev. D* **24** (1981) 450.
- [3] J.D. Bjorken, *Highly relativistic nucleus-nucleus collisions: The central rapidity region*, *Phys. Rev. D* **27** (1983) 140.

- [4] M. Gyulassy and L. McLerran, *New forms of qcd matter discovered at rhic*, *Nucl. Phys. A* **750** (2005) 30 .
- [5] STAR Collaboration, *Experimental and theoretical challenges in the search for the quark-gluon plasma: The star collaboration's critical assessment of the evidence from rhic collisions*, *Nucl. Phys. A* **757** (2005) 102 .
- [6] PHENIX Collaboration, *Formation of dense partonic matter in relativistic nucleus-nucleus collisions at rhic: Experimental evaluation by the phenix collaboration*, *Nucl. Phys. A* **757** (2005) 184 .
- [7] ALICE Collaboration, *Elliptic flow of charged particles in pb-pb collisions at $\sqrt{s_{NN}} = 2.76$ TeV*, *Phys. Rev. Lett.* **105** (2010) 252302.
- [8] ATLAS Collaboration, *Measurement of the pseudorapidity and transverse momentum dependence of the elliptic flow of charged particles in lead-lead collisions at $\sqrt{s_{NN}} = 2.76$ tev with the atlas detector*, *Phys. Lett. B* **707** (2012) 330 .
- [9] CMS Collaboration, *Centrality dependence of dihadron correlations and azimuthal anisotropy harmonics in pppb collisions at $\sqrt{s_{NN}} = 2.76$ TeV*, *Eur. Phys. J. C* **72** (2012) 10052.
- [10] CMS Collaboration, *Observation of long-range, near-side angular correlations in pppb collisions at the lhc*, *Phys. Lett. B* **718** (2013) 795 .
- [11] PHENIX Collaboration, *Creation of quark-gluon plasma droplets with three distinct geometries*, *Nat. Phys.* **15** (2019) 214.
- [12] M. Braun, J. Dias de Deus, A. Hirsch, C. Pajares, R. Scharenberg and B. Srivastava, *De-confinement and clustering of color sources in nuclear collisions*, *Phys. Rep.* **599** (2015) 1 .
- [13] I. Bautista, C. Pajares and J.E. Ramírez, *String percolation in aa and p+ p collisions*, *Rev. Mex. Fis.* **65** (2019) 197.
- [14] M.A. Braun and C. Pajares, *Implications of color-string percolation on multiplicities, correlations, and the transverse momentum*, *Eur. Phys. J. C* **16** (2000) 349.
- [15] N. Armesto, M.A. Braun, E.G. Ferreira and C. Pajares, *Percolation approach to quark-gluon plasma and J/ψ suppression*, *Phys. Rev. Lett.* **77** (1996) 3736.
- [16] P. Tribedy and R. Venugopalan, *Saturation models of HERA DIS data and inclusive hadron distributions in p+p collisions at the LHC*, *Nucl. Phys. A* **850** (2011) 136.
- [17] P. Tribedy and R. Venugopalan, *QCD saturation at the LHC: Comparisons of models to p + p and A + A data and predictions for p + Pb collisions*, *Phys. Lett. B* **710** (2012) 125.
- [18] J.E. Ramírez, B. Díaz and C. Pajares, *Interacting color strings as the origin of the liquid behavior of the quark-gluon plasma*, *Phys. Rev. D* **103** (2021) 094029.
- [19] T. Aste and T. di Matteo, *2 - nanometric architectures: emergence of efficient non-crystalline atomic organization in nanostructures*, in *Nanostructure Control of Materials*, R. Hannink and A. Hill, eds., pp. 32–56, Woodhead Publishing (2006), <https://www.sciencedirect.com/science/article/pii/B9781855739338500026>.
- [20] J. Dias de Deus, A.S. Hirsch, C. Pajares, R.P. Scharenberg and B.K. Srivastava, *Transport coefficient to trace anomaly in the clustering of color sources approach*, *Phys. Rev. C* **93** (2016) 024915.
- [21] P. Sahoo, S.K. Tiwari, S. De, R. Sahoo, R.P. Scharenberg and B.K. Srivastava, *Thermodynamic and transport properties in au + au collisions at rhic energies from the clustering of color strings*, *Mod. Phys. Lett. A* **34** (2019) 1950034.

- [22] J.C. Texca García, D. Rosales Herrera, J.E. Ramírez, A. Fernández Téllez and C. Pajares, *Percolation leads to finite-size effects on the transition temperature and center-of-mass energy required for quark-gluon plasma formation*, *Phys. Rev. D* **106** (2022) L031503.
- [23] N.S. Amelin, M.A. Braun and C. Pajares, *Multiple production in the Monte Carlo string fusion model*, *Phys. Lett. B* **306** (1993) 312.
- [24] J. Dias de Deus and C. Pajares, *Percolation of color sources and critical temperature*, *Phys. Lett. B* **642** (2006) 455 .
- [25] D. Chandler, *Introduction to Modern Statistical Mechanics*, Oxford University Press, New York (1987).
- [26] V. Myroshnychenko and C. Brosseau, *Possible manifestation of nonuniversality in some continuum percolation systems*, *J. Phys. D* **41** (2008) 095401.
- [27] V. Myroshnychenko and C. Brosseau, *Effective complex permittivity and continuum percolation analysis of two-phase composite media*, *IEEE Trans. Dielectr. Electr. Insul.* **16** (2009) 1209.
- [28] B.I. Halperin, S. Feng and P.N. Sen, *Differences between lattice and continuum percolation transport exponents*, *Phys. Rev. Lett.* **54** (1985) 2391.
- [29] S. Mertens and C. Moore, *Continuum percolation thresholds in two dimensions*, *Phys. Rev. E* **86** (2012) 061109.
- [30] J.L. Albacete and C. Marquet, *Gluon saturation and initial conditions for relativistic heavy ion collisions*, *Prog. Part. Nucl. Phys.* **76** (2014) 1.
- [31] L.V. Gribov, E.M. Levin and M.G. Ryskin, *Semihard Processes in QCD*, *Phys. Rept.* **100** (1983) 1.
- [32] A.H. Mueller, *Small x Behavior and Parton Saturation: A QCD Model*, *Nucl. Phys. B* **335** (1990) 115.
- [33] J.P. Blaizot and A.H. Mueller, *The Early Stage of Ultrarelativistic Heavy Ion Collisions*, *Nucl. Phys. B* **289** (1987) 847.
- [34] L.D. McLerran and R. Venugopalan, *Green's functions in the color field of a large nucleus*, *Phys. Rev. D* **50** (1994) 2225.
- [35] I. Balitsky, *Operator expansion for high-energy scattering*, *Nucl. Phys. B* **463** (1996) 99.
- [36] Y.V. Kovchegov, *Small x $F(2)$ structure function of a nucleus including multiple pomeron exchanges*, *Phys. Rev. D* **60** (1999) 034008.
- [37] J. Jalilian-Marian, A. Kovner, A. Leonidov and H. Weigert, *The Wilson renormalization group for low x physics: Towards the high density regime*, *Phys. Rev. D* **59** (1998) 014014.
- [38] J. Jalilian-Marian, A. Kovner, A. Leonidov and H. Weigert, *The BFKL equation from the Wilson renormalization group*, *Nucl. Phys. B* **504** (1997) 415.
- [39] E. Iancu, A. Leonidov and L.D. McLerran, *The Renormalization group equation for the color glass condensate*, *Phys. Lett. B* **510** (2001) 133.
- [40] E. Iancu, A. Leonidov and L.D. McLerran, *Nonlinear gluon evolution in the color glass condensate. 1.*, *Nucl. Phys. A* **692** (2001) 583.
- [41] H. Weigert, *Unitarity at small Bjorken x* , *Nucl. Phys. A* **703** (2002) 823.
- [42] A. Dumitru, D.E. Kharzeev, E.M. Levin and Y. Nara, *Gluon Saturation in pA Collisions at the LHC: KLN Model Predictions For Hadron Multiplicities*, *Phys. Rev. C* **85** (2012) 044920.
- [43] A. Dumitru and Y. Nara, *KNO scaling of fluctuations in pp and pA, and eccentricities in heavy-ion collisions*, *Phys. Rev. C* **85** (2012) 034907.

- [44] H. Kowalski and D. Teaney, *An Impact parameter dipole saturation model*, [*Phys. Rev. D* **68** \(2003\) 114005](#).
- [45] B. Schenke, P. Tribedy and R. Venugopalan, *Fluctuating Glasma initial conditions and flow in heavy ion collisions*, [*Phys. Rev. Lett.* **108** \(2012\) 252301](#).
- [46] B. Schenke, P. Tribedy and R. Venugopalan, *Event-by-event gluon multiplicity, energy density, and eccentricities in ultrarelativistic heavy-ion collisions*, [*Phys. Rev. C* **86** \(2012\) 034908](#).
- [47] L.D. McLerran and R. Venugopalan, *Computing quark and gluon distribution functions for very large nuclei*, [*Phys. Rev. D* **49** \(1994\) 2233](#).
- [48] L.D. McLerran and R. Venugopalan, *Gluon distribution functions for very large nuclei at small transverse momentum*, [*Phys. Rev. D* **49** \(1994\) 3352](#).
- [49] F. Gelis, E. Iancu, J. Jalilian-Marian and R. Venugopalan, *The Color Glass Condensate*, [*Ann. Rev. Nucl. Part. Sci.* **60** \(2010\) 463](#).
- [50] B. Schenke, P. Tribedy and R. Venugopalan, *Multiplicity distributions in p+p, p+A and A+A collisions from Yang-Mills dynamics*, [*Phys. Rev. C* **89** \(2014\) 024901](#).
- [51] C. Gale, S. Jeon, B. Schenke, P. Tribedy and R. Venugopalan, *Event-by-event anisotropic flow in heavy-ion collisions from combined Yang-Mills and viscous fluid dynamics*, [*Phys. Rev. Lett.* **110** \(2013\) 012302](#).
- [52] K. Dusling and R. Venugopalan, *Azimuthal collimation of long range rapidity correlations by strong color fields in high multiplicity hadron-hadron collisions*, [*Phys. Rev. Lett.* **108** \(2012\) 262001](#).
- [53] L. McLerran and P. Tribedy, *Intrinsic Fluctuations of the Proton Saturation Momentum Scale in High Multiplicity p+p Collisions*, [*Nucl. Phys. A* **945** \(2016\) 216](#).
- [54] B. Schenke, C. Shen and P. Tribedy, *Running the gamut of high energy nuclear collisions*, [*Phys. Rev. C* **102** \(2020\) 044905](#).
- [55] Y.V. Kovchegov, *NonAbelian Weizsacker-Williams field and a two-dimensional effective color charge density for a very large nucleus*, [*Phys. Rev. D* **54** \(1996\) 5463](#).
- [56] D. Kharzeev, E. Levin and M. Nardi, *Color glass condensate at the LHC: Hadron multiplicities in pp, pA and AA collisions*, [*Nucl. Phys. A* **747** \(2005\) 609](#).
- [57] D. Kharzeev and M. Nardi, *Hadron production in nuclear collisions at RHIC and high density QCD*, [*Phys. Lett. B* **507** \(2001\) 121](#).
- [58] P. Sahoo, S.K. Tiwari and R. Sahoo, *Electrical conductivity of hot and dense qcd matter created in heavy-ion collisions: A color string percolation approach*, [*Phys. Rev. D* **98** \(2018\) 054005](#).
- [59] P. Sahoo, R. Sahoo and S.K. Tiwari, *Wiedemann-franz law for hot qcd matter in a color string percolation scenario*, [*Phys. Rev. D* **100** \(2019\) 051503](#).
- [60] J.E. Ramírez and C. Pajares, *Area covered by disks in small-bounded continuum percolating systems: An application to the string percolation model*, [*Phys. Rev. E* **100** \(2019\) 022123](#).
- [61] PARTICLE DATA GROUP collaboration, *Review of Particle Physics*, [*Chin. Phys. C* **40** \(2016\) 100001](#).